Supplementary Information for

Spatial and temporal expansion of global fire activity in response to climate change

Martín Senande-Rivera[1*], Damián Insua-Costa[1] and Gonzalo Miguez-Macho[1].

[1]Nonlinear Physics Group, Faculty of Physics, Universidade de Santiago de Compostela, Galicia, Spain.

[*]Correspondence to: martin.senande.rivera@usc.es

Fire season and croplands

The fire season length (FSL) is defined as the minimum number of consecutive months that contain more than 80% of the annual burned area. This definition is widely used[13,62,63]. If there are multiple combinations of the same number of months with more than 80% of the annual burned area, the combination corresponding to the maximum value of burned area is selected as the fire season (FS). Fig. S1a shows the FSL obtained from GFED4 burned area data, using monthly means.

The GFED4 dataset[19] contains information about the land cover distribution within the burned area. Fig. S1b shows the percentage of the mean annual burned area (BA) associated to croplands (one of the land cover categories of the GFED4 data). Fires on agricultural land can correspond to human-controlled agricultural practices, with minimal relationship to weather or climate conditions.

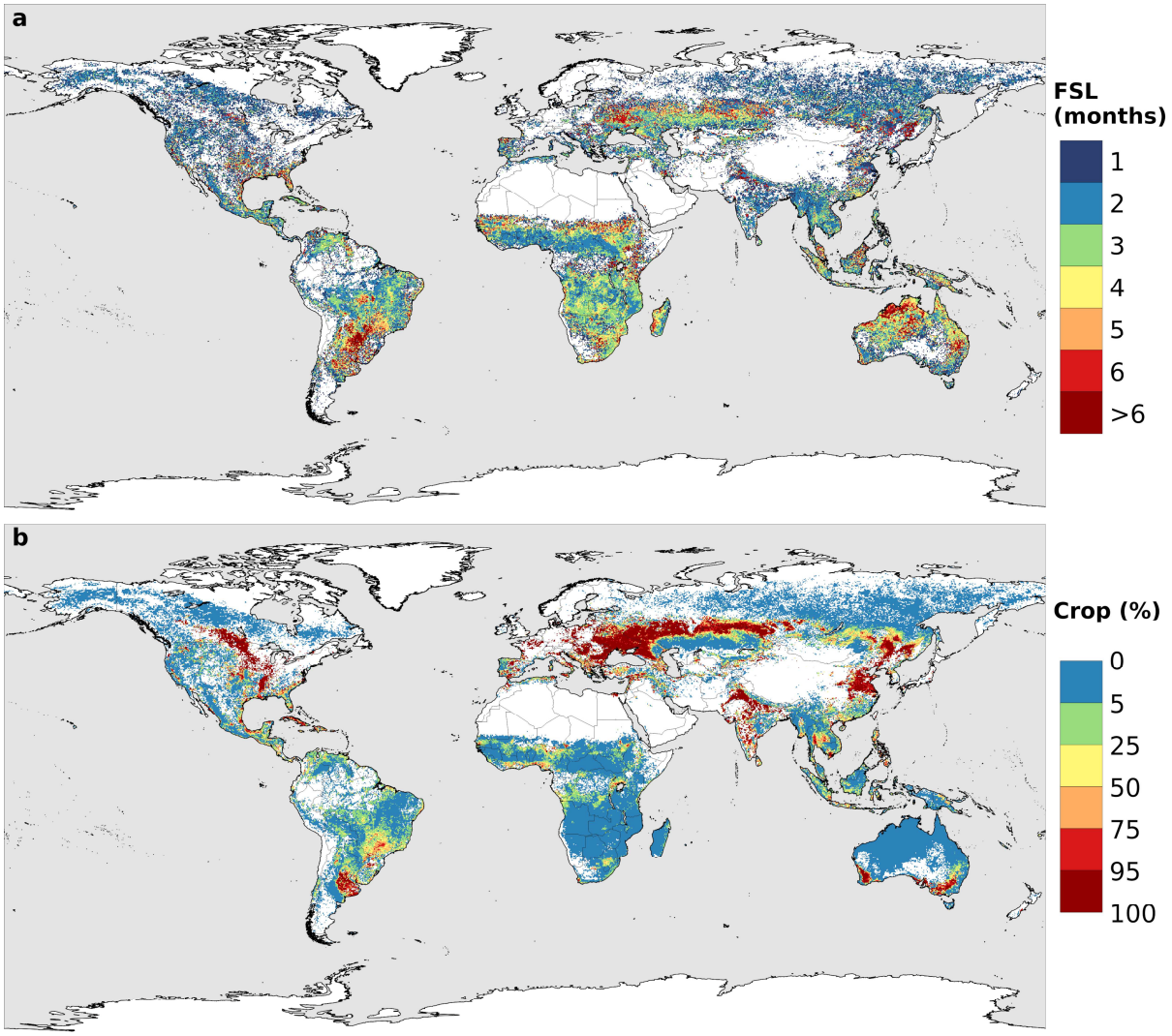

Figure S1. a, Fire season length. **b**, Percentage of mean annual burned area (BA) corresponding to cropland land cover from GFED4 data[19].

Threshold selection

We sort out global grid points with burned area data into 5 different groups according to their main Köppen-Geiger climate class[20]: tropical (A), arid (B), temperate (C), cold (D) and polar (E). We follow the classification criteria used by Beck et al.[34] and Peel et al.[64], but with a new threshold between temperate (C) and cold (D) climates. Since the definition of the Köppen-Geiger climate classification several authors proposed changes, and most of these proposals were aimed at improving the C-D boundary[65], such as redefining the coolest-month isotherm at 0°C[34,64,66] or -3°C[67]. We modified the C-D boundary to associate the cold climate (D) to the boreal forest (taiga), so we set the threshold between temperate and cold climates at 2°C of

mean annual temperature (MAT). This threshold is consistent with Whittaker[68] and Woodward et al.[69], who determine the temperate-boreal forest transition to occur below 5°C of mean annual temperature. Fig. S2 shows the Köppen-Geiger world classification with this modification, computed from WFDE5 climate data[55].

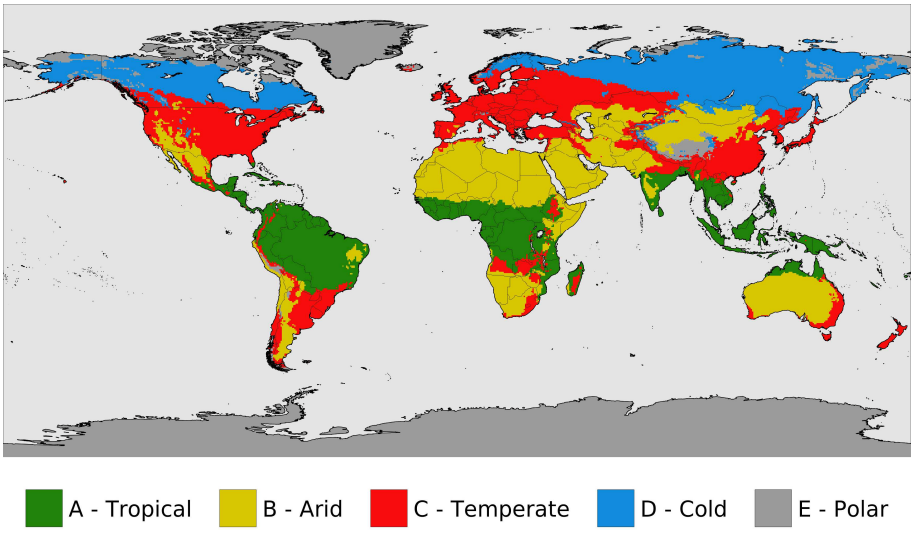

Figure S2. World general climate classification. Based on the Köppen-Geiger classification but modifying the C-D category threshold to delimit the boreal forest ecoregion.

We examine next the statistical distribution of different climatic variables at fire-impacted and fireless pixels within the Köppen-Geiger main categories, to find the conditions that are suitable for fire activity. The objective is to obtain sets of climatic thresholds that univocally identify the different classes of burned areas in actual fire occurrence data, both in extent and duration of the FS. Precisely, for each main Köppen-Geiger category (Fig. S2) we compare the values of variables MAP, MAT, Pmin and Tmax in fire-prone regions (locations with BA≥100 ha), against values in non-fire regions (locations with BA<100 ha). For the monthly variables Pm and Tm, we compare their magnitude during the months of the FS in places with BA≥100 ha (which we will refer to as "fire points") against the remaining monthly data (i.e. "non fire points": all monthly values at locations with BA<100 ha and values in months that do not belong to the FS in places with BA≥100 ha). We excluded from the statistical distributions data from the fire-prone regions with a cropland land cover percentage of more than 90% (Fig. S1b), due to the likely relation of fires with agricultural practices in these places[70,71]. Fig. S3, S4, S11 and S12 show all the statistical distributions.

We set thresholds in those variables that show a different behaviour between the values associated with high fire activity and the values that are not. The thresholds are selected automatically at the value that maximizes the area enclosed between the density function of the points with high fire activity and the density function of the points without fire activity (coloured areas in Fig. S3, S4, S11 and S12). In an ideal scenario where the data points with fire activity were perfectly separated from the remaining points, this area would be equal to 1. In most cases, however, it is the simultaneous meeting of the conditions for two variables that determines fire risk, thus, there can be a sizeable amount of non-fire data points satisfying either of them. The objective is then that fire points, and especially those representing locations and months with more burned area, fulfil all the conditions simultaneously in the highest percentage possible, while non-fire points that do so are a minority. The obtained thresholds are rounded to easy-to-use values. Tab. S1 shows the selected threshold values, the percentage of data points that meet the thresholds and the burned area share they represent.

Table S1. Threshold selection data. Fire point percentage indicates the percentage of points with fire activity (color lines in the statistical distributions) that meet the threshold. Non fire point percentage indicates the percentage of points without fire activity (black lines in the statistical distributions) that meet the threshold. BA percentage indicates the percentage of burned area associated with the points that meet the threshold. The uncertity in the obtained threshold is the size of the x-axis discretization used in the calculation. For the monthly variables, "points" refer to monthly values at any location.

	Variable	Fire point percentage	Non-fire point percentage	BA percentage	Obtained threshold	Selected threshold
A - ds	Pm	83.0%	27.3%	95.9%	84.6±3.1 mm	85 mm
	Pmin	79.1%	29.4%	95.6%	20.9±2.0 mm	20 mm
B - dhs	MAP	90.2%	30.1%	97.8%	223.6±4.3 mm	225 mm
	Tm	83.2%	58.9%	90.0%	19.1±0.5 °C	19 °C
C - dhs	Pm	55.9%	25.2%	85.5%	41.5±3.1 mm	40 mm
	Tm	86.8%	49.2%	94.3%	12.0±0.5 °C	12 °C
D - hs	Tm	85.5%	26.7%	76.3%	6.9±0.5 °C	7 °C
	Tmax	72.1%	42.6%	80.6%	14.7±0.1 °C	15 °C

Tropical dry season fire category

Fire activity in the Tropics is confined to relatively dry months, in which the mean monthly precipitation (Pm) is less than 85 mm (Fig. S3a). This variable is the one presenting more differences between the fire-prone and the non-fire probability density functions (Fig. S3a). As shown in Tab. S1, as many as 83% of the points with high fire activity, but only 27% of the non-fire points, are to the left of the threshold.

The statistical distribution of Pmin (Fig. S3c) indicates that under tropical climates, fire activity occurs in places where at least one month is extremely dry (< 20 mm). This implies that places where the dry season consists of months with mean monthly precipitations ranging between 20 mm and 85 mm, will not be classified as fire-prone. A stronger precipitation seasonality is needed, where at least one month has a mean precipitation under 20 mm. If this Pmin threshold is satisfied, the number of months with Pm < 85mm is defined as the potential fire season (PFS) under tropical climates. The Pmin threshold is consistent with Cahoon et al.[21], who showed that the peak burning activity month in the savannas north of the Equator receives less than 25 mm of precipitation.

The MAP statistical distribution (Fig. S3e) shows that fire-prone areas have relatively lower annual precipitations than the non-fire-prone regions; however, since this is likely due to the aforementioned rainfall seasonality, we find that we do not need to use an upper MAP limit to characterize the fire-prone regions in the Tropics. Neither we need to employ temperature variables in the fire-climate classification, as they do not show any distinct behaviour in the fire season (Fig. S3b,d,f).

The strong link between fires in the Tropics and rainfall seasonality has been widely studied[21-23]. The location of the Inter-Tropical Convergence Zone (ITCZ) generally determines the precipitation patterns in the Tropics, and consequently the fire activity[23].

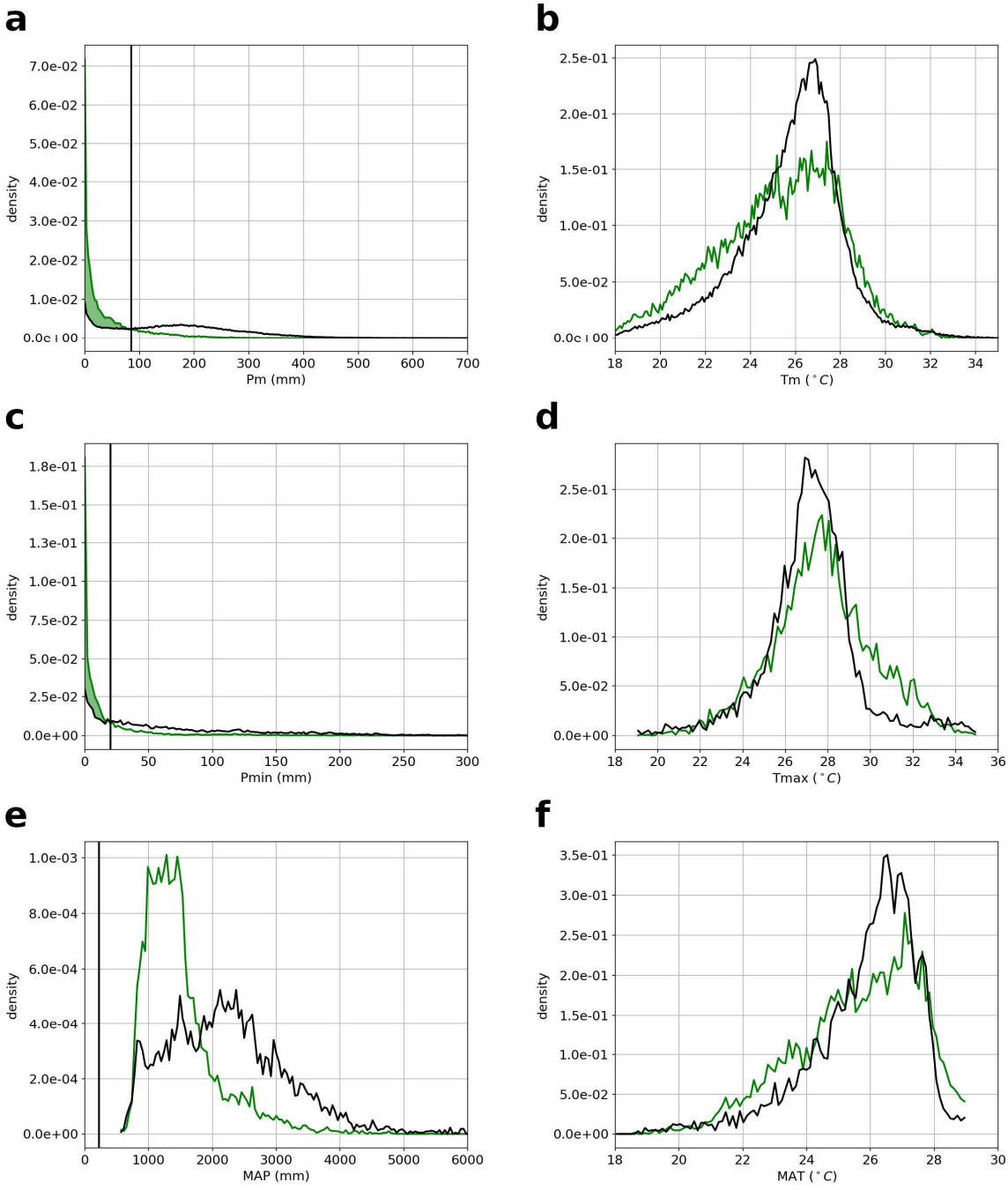

Figure S3. Tropical statistical distributions. Monthly precipitation (Pm), monthly temperature (Tm), precipitation of the driest month (Pmin), temperature of the hottest month (Tmax), mean annual precipitation (MAP) and mean annual temperature (MAT) probability density functions. For annual variables (Pmin, Tmax, MAP and MAT), green distributions represent spatial points with BA≥100 ha, and black distributions represent the remaining tropical points. For monthly variables (Pm and Tm), green distributions show monthly values of the FS of places with BA≥100 ha, and black distributions represent the remaining tropical monthly data. The selected thresholds are indicated through black vertical lines.

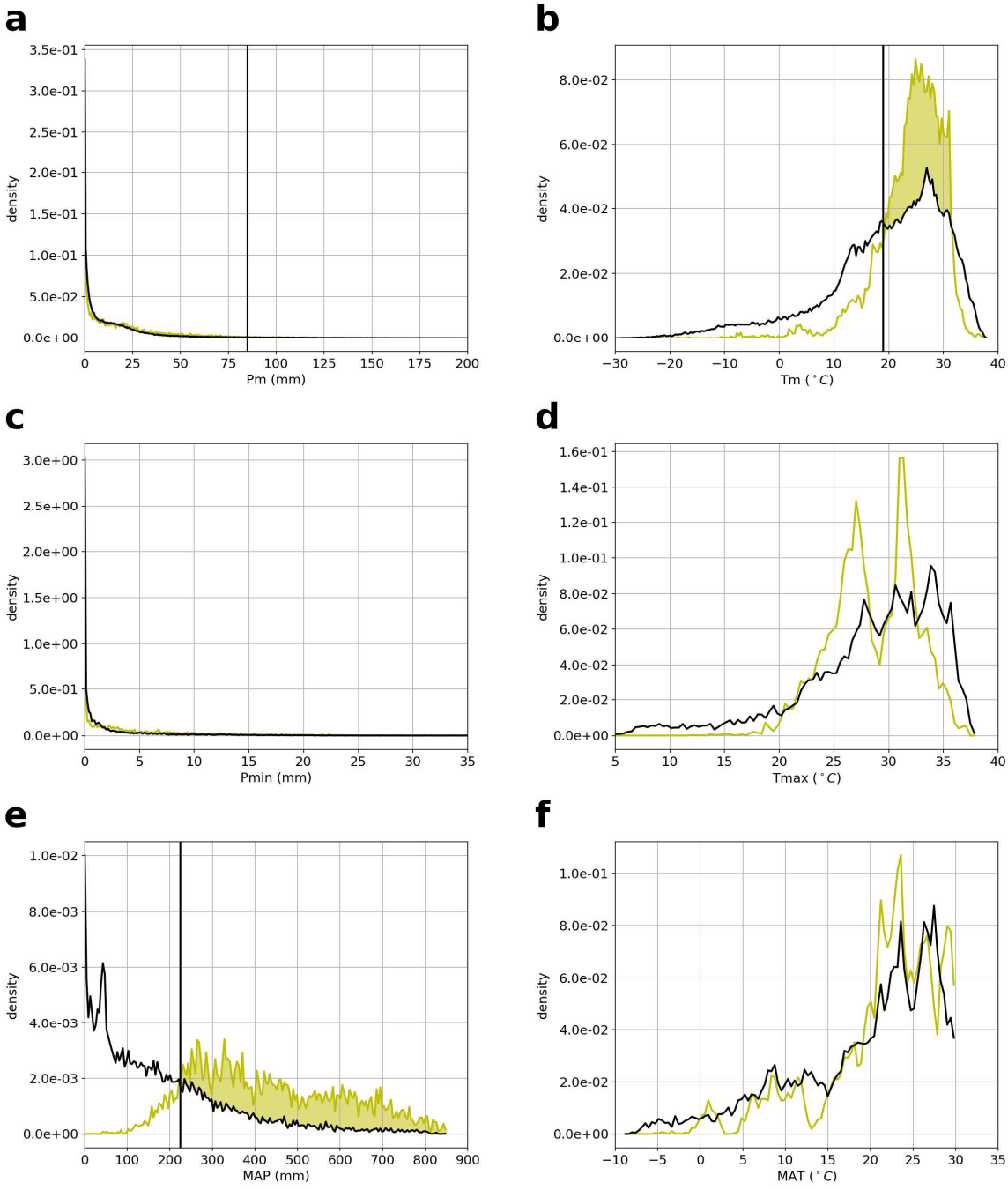

Figure S4. Arid statistical distributions. Same as Fig. S3 but with arid data. Fire-prone probability density functions are shown in yellow.

Arid dry and hot season fire category

An arid dry and hot season fire category (B-dhs) is initially defined through a MAP (Fig. S4e) and a Tm threshold (Fig. S4b). Fires are observed in regions with an annual precipitation that enables the existence of a certain amount of vegetation, so fire in dry climates is more limited

by fuel amount than by the fuel moisture[72,73]. Fig. S4e shows that fire-prone arid areas have an annual precipitation higher than 225 mm. This threshold is applied to all other categories (Fig. S3e, S11e and S12e) to analyse the possible future desertification due to climate change.

High monthly temperatures are also related to fire activity. Fig. S4b shows that most of the fire season months in arid climates have temperatures above 19°C. Despite monthly precipitation distributions not showing significant differences between fire-prone and non-fire-prone data, we also include a Pm threshold of 85 mm (near the 95th percentile of the fire points distribution: 85.5 mm) in order to detect a possible fire season shortening due to a future precipitation increase (Fig. S4a). Above this monthly precipitation value, the number of months belonging to a fire season anywhere with arid climate is almost negligible.

However, these three thresholds (MAP, Tm and Pm) are not enough to characterize the fire season in certain regions. We checked the monthly values of burned area, precipitation and temperature in different fire-prone arid regions (Fig. S5, S6, S7 and S8) and found that the fire season is associated with a hot season in midlatitude arid areas where no clear wet period is observed, e.g. Kazakhstan and North America (Fig. S5 and S6), but closer to the tropics where it is warm year-round, it can be also determined by the existence of a pronounced annual wet and dry season cycle, with fires occurring sometime during the dry season, in places just at the beginning (e.g. Sahel region, Fig. S8) while in others, more toward the end of it (e.g. Botswana and Australia, Fig. S7 and S8).

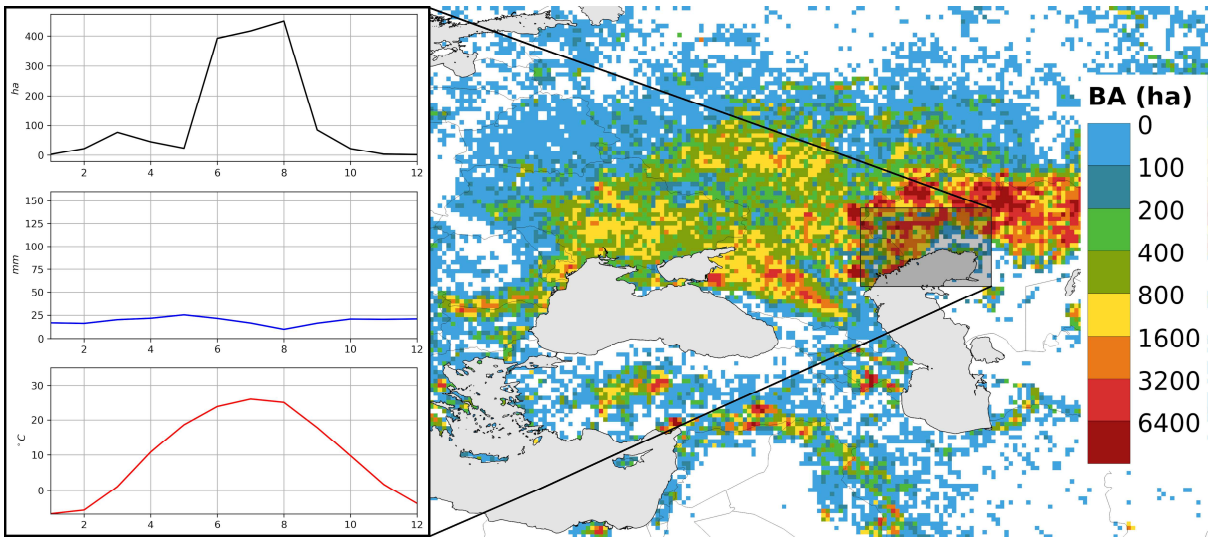

Figure S5. Mean monthly values for Asian arid fire-prone regions (BA>0ha). Mean monthly burned area in black, precipitation in blue and 2m air temperature in red.

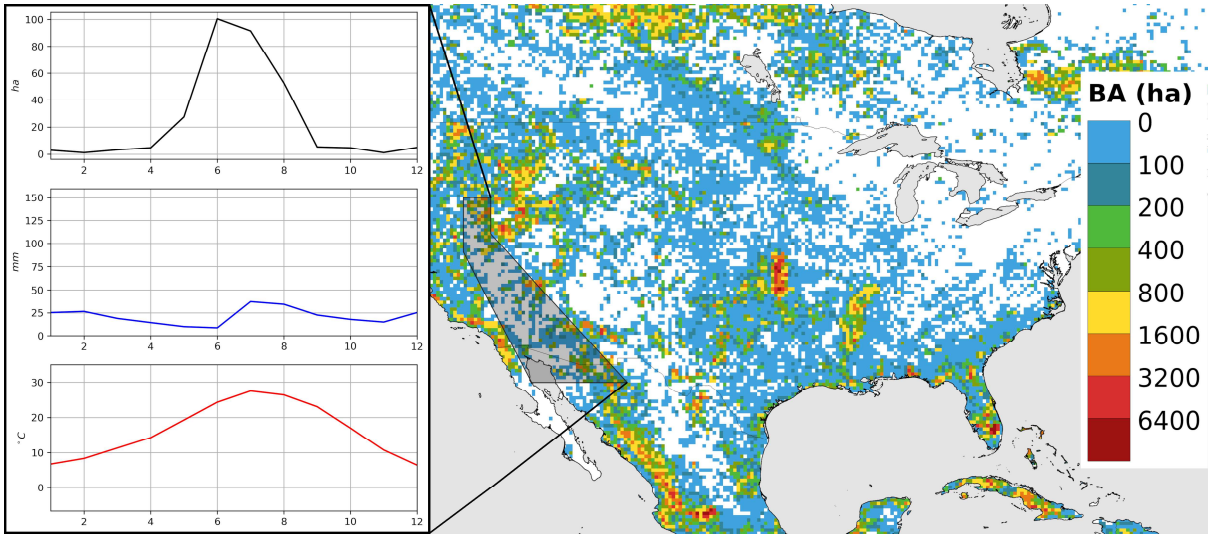

Figure S6. Mean monthly values for North American arid fire-prone regions (BA>0ha). Mean monthly burned area in black, precipitation in blue and 2m air temperature in red.

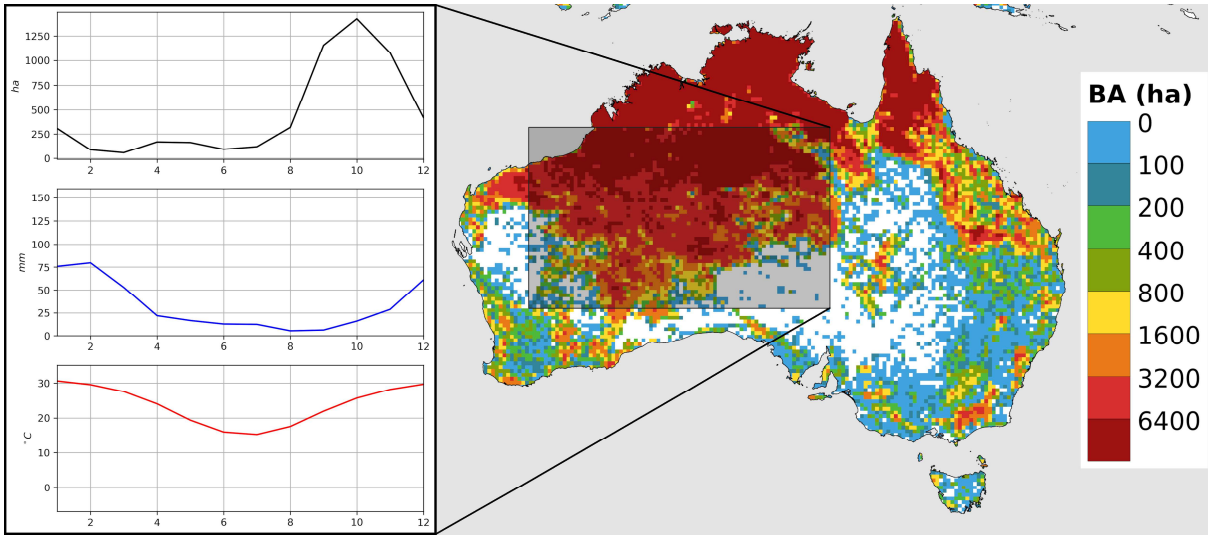

Figure S7. Mean monthly values for Australian arid fire-prone regions (BA>0ha). Mean monthly burned area in black, mean monthly precipitation in blue and mean monthly 2m air temperature in red.

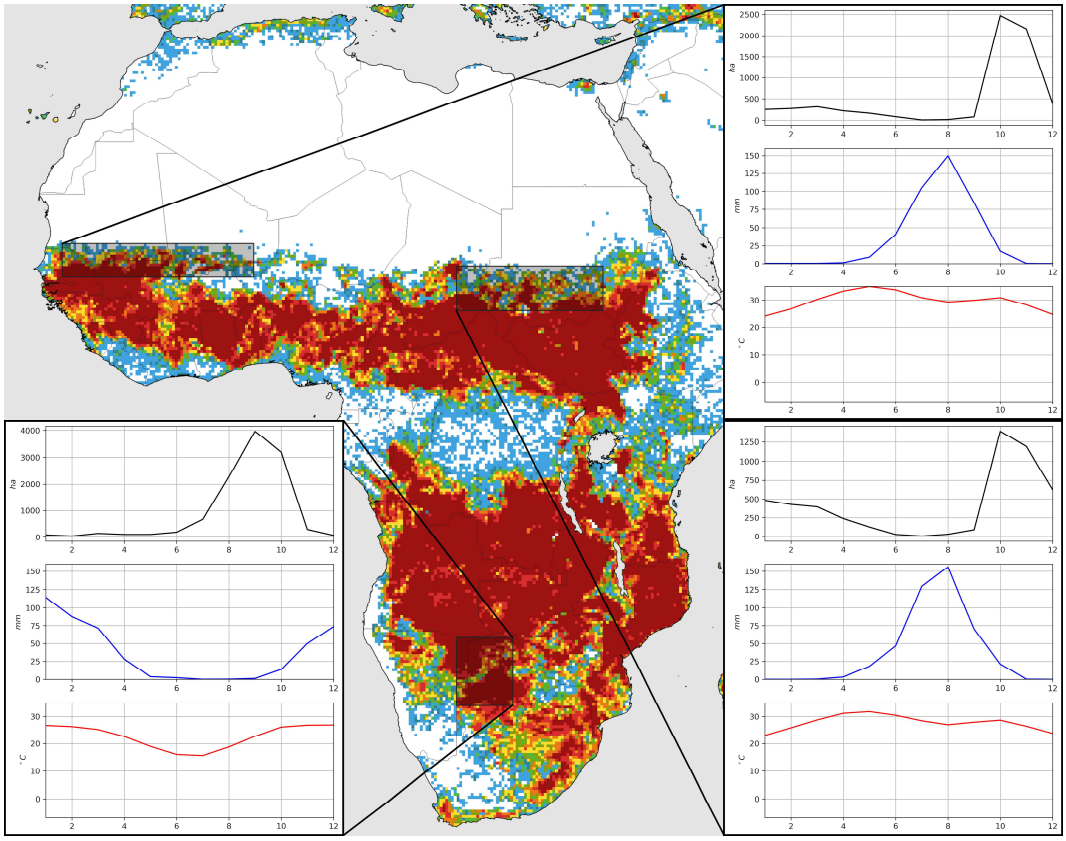

Figure S8. Mean monthly values of African fire-prone arid regions (BA>0ha). Mean monthly burned area in black, mean monthly precipitation in blue and mean monthly 2m air temperature in red.

Fig. S9 shows the distance in months between the month of maximum burned area and the wettest month (Fig. S9a), and between the month of maximum burned area and the hottest month (Fig. S9b). The values of the latter variables indicate that the maximum burned area in the cool arid regions (e.g. Kazakhstan and North America) is reached during the hottest months, so that the Tm threshold can be sufficient to define the fire season. However, in warmer regions with more tropical monsoonal climatic features, additional variables must be considered. Fig. S10a compares the MAT probability density function of areas where the month of maximum burned area precede the wettest month, i.e., it is at the end of the dry season (yellow distribution) vs. areas where the month of maximum burned area follows the wettest month, i.e., it is at the beginning of the dry season (orange distribution). According to this, we define three different arid fire-prone regions:

(a) MAT < 18°C. Due to the practical absence of precipitation seasonality (Fig. S5 and S6), the fire season coincides with the hot season (Fig. S10b).

(b) 18°C ≤ MAT < 27°C. The fire season occurs at the end of the dry months, just before the wet season, when the fuel moisture reaches the lowest values (Fig. S10c). For this MAT interval we will constrain the fire season to the four months at the end of the dry season.

(c) MAT ≥ 27°C. The high temperatures rapidly dry the fuel, so the fire season occurs at the beginning of the dry season, right after the wet season (Fig. S10d). Two more factors enhance the rapid fuel drying in the Sahel region, the low soil water retention[71] and the grass-dominated vegetation[74] in contrast with other arid regions covered mostly by shrubs or hummock grasses, as in Australia. The herbaceous vegetation desiccates early in the dry season[75], favouring fires, while the severe drought suppresses grass production at the end of the dry season, limiting fires[75]. In addition, fires in the early dry season are used as preventive burning strategies in order to hinder later destructive fires in Mali[76] and Senegal[77]. Therefore, for these MAT values we will constrain the fire season to the five months at the beginning of the dry season.

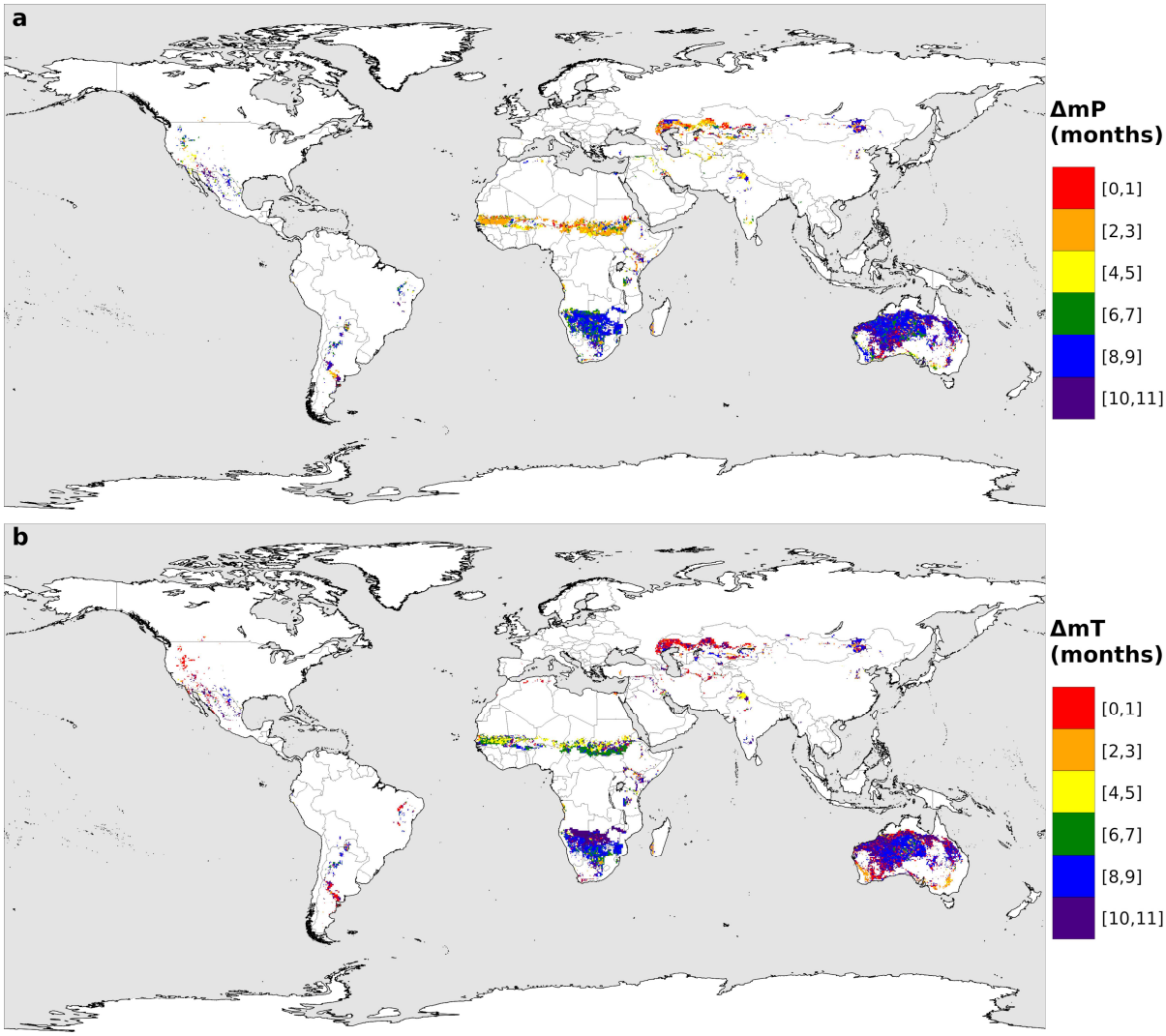

Figure S9. Months from the month with highest burned area. a, Time period in months between the month with most burned area and the wettest month (ΔmP). **b**, Time period in months between the month with most burned area and the hottest month (ΔmT).

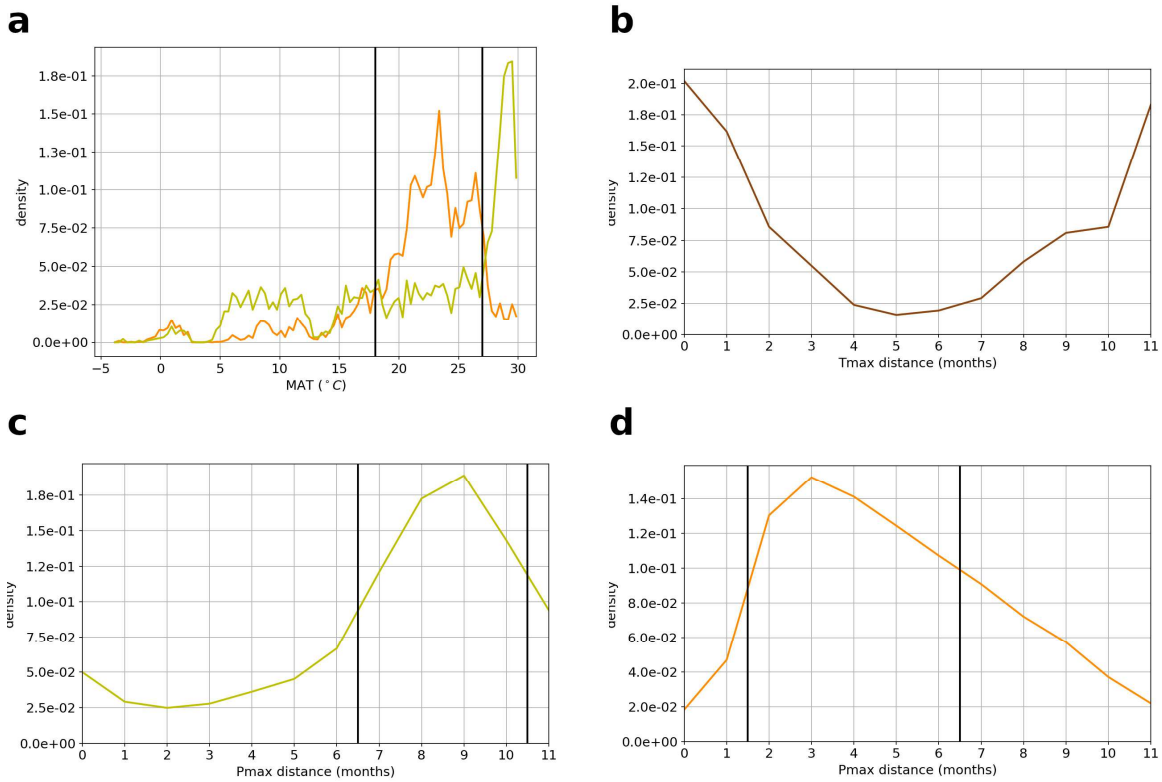

177

178 **Figure S10. Auxiliar statistical distributions for arid climates. a,** MAT probability density
179 function of arid fire-prone points (BA≥100 ha) with ΔmP>6, i.e. with more than 6 months in
180 between the month with most burned area and the wettest month (yellow) and with ΔmP≤6
181 values (orange). **b,** For points with MAT < 18°C, probability density function of the distance
182 in months between fire season months and the hottest month (brown). **c,** For points with 18°C
183 ≤ MAT < 27°C, probability density function of the distance in months between fire season
184 months and the wettest month (yellow). **d,** For points with MAT ≥ 27°C, probability density
185 function of the distance in months between fire season months and the wettest month (orange).

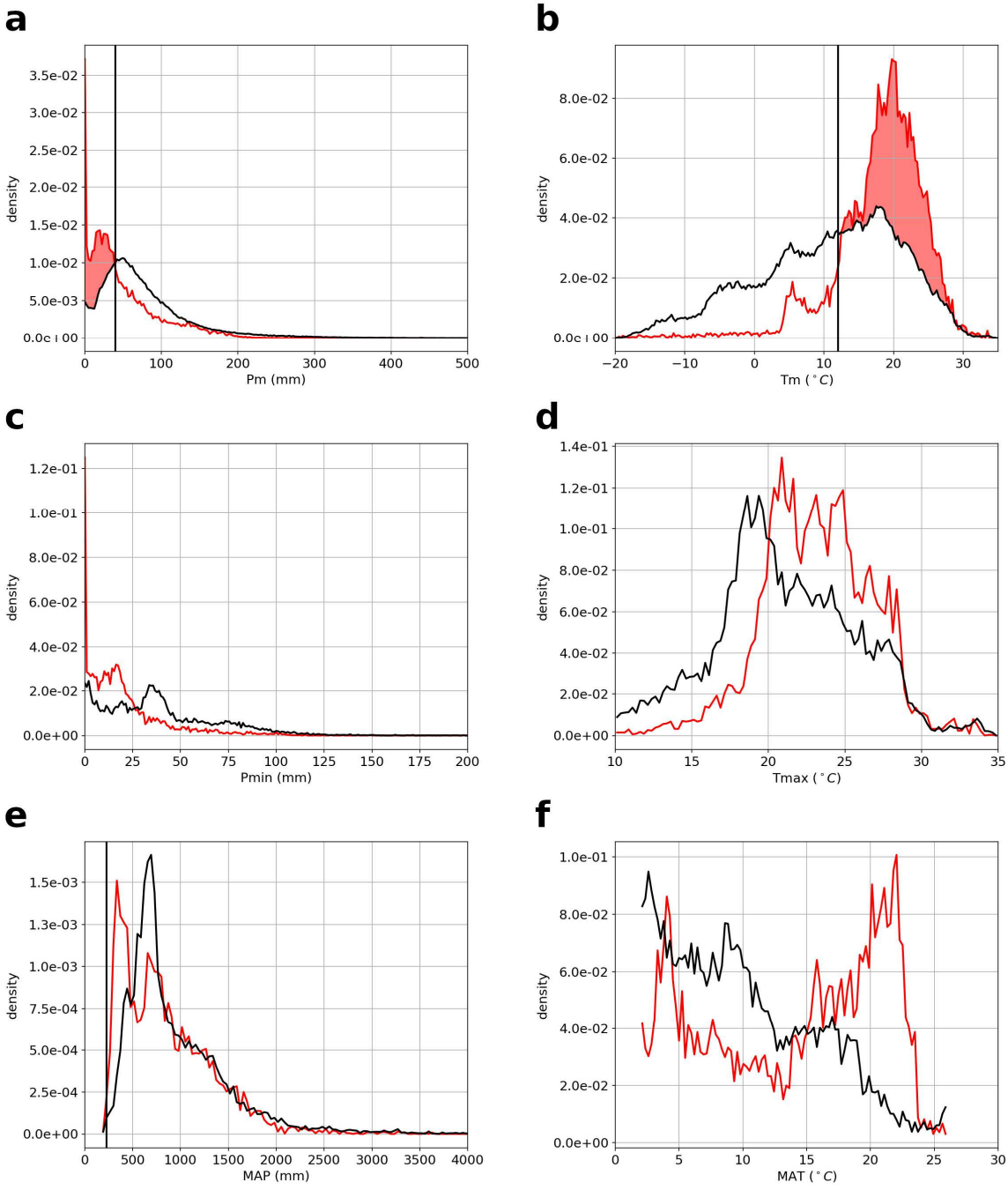

186

187 **Figure S11. Temperate statistical distributions.** Same as Fig. S3 but with temperate data.
188 Fire-prone probability density functions are shown in red.

189 *Temperate dry and hot season fire category*

190 The Temperate dry and hot season fire category (C-dhs) is defined by setting a Pm and a Tm
191 threshold. The fire season months are relatively dry; most of the Pm values are concentrated
192 below a 40 mm threshold (Fig. S11a), with a pronounced peak close to 0 mm, meaning a totally

dry month. The Tm distribution (Fig. S11b) shows also significant differences between fire season months and non-fire-prone months, indicating that cooler monthly temperature values below 12°C tend to hamper fire activity. Therefore, the fire season in temperate climates occurs during dry and hot conditions.

Unlike in ever warm tropical climates, where fire risk is largely determined by the lack of precipitation in the dry season, in midlatitude temperate climates with temperature seasonality, fires occur when dry conditions coincide with the warm season[26-31], as cold temperatures diminish fire risk. Thus, the use of simultaneous monthly precipitation and temperature thresholds are needed. The mean annual MAT and MAP statistical distributions (Fig. S11e,f) do not show any important distinction in temperate fire-prone regions. Even so, we use a lower 225 mm MAP threshold to take into account a possible future desertification.

Boreal hot season fire category

The Boreal hot season fire category (D-hs) is mainly defined through a Tmax and a Tm threshold, given that the fire season is characterized by the warmest conditions along the year. Fig. S12b clearly shows how most fire season months have monthly temperatures above 7°C. In a similar way as we did for the precipitation thresholds in Tropical climates, we combine this monthly threshold with a maximum monthly temperature threshold of 15°C (Fig. S12d). This indicates that boreal regions with a warm season with more moderate monthly temperatures ranging between 7°C and 15°C are not classified as fire prone.

The monthly precipitation statistical distribution (Fig. S12a) indicates that the fire season under Boreal climates is wetter than the rest of the year. This characteristic of the fire season is counter-intuitive because high rainfall during the fire season does not enhance fire activity. However, it is typical of boreal climates to present higher precipitation in warm months, as the very cold air masses in winter contain little moisture and precipitation amounts are commonly small, especially in regions away from the coast. Therefore, we do not use a lower limit for monthly precipitation, and instead, we set an upper threshold of 110 mm (near the 95th percentile of the fire point distribution: 113 mm) to consider a possible future decrease in fire activity due to a monthly precipitation increase during the fire season (Fig. S12a).

Due to the practical absence of polar (E) fires, as cold temperatures are registered year around and vegetation consists of tundra, we excluded this general climate class from our analysis.

Tab. 1 show all defining criteria for the four classes, including the Köppen-Geiger-based general classification of climates zones and the specific fire classification thresholds. One spatial point is classified as fire-prone if at least one month meets all the conditions. The months that meet the thresholds conform the potential fire season (PFS).

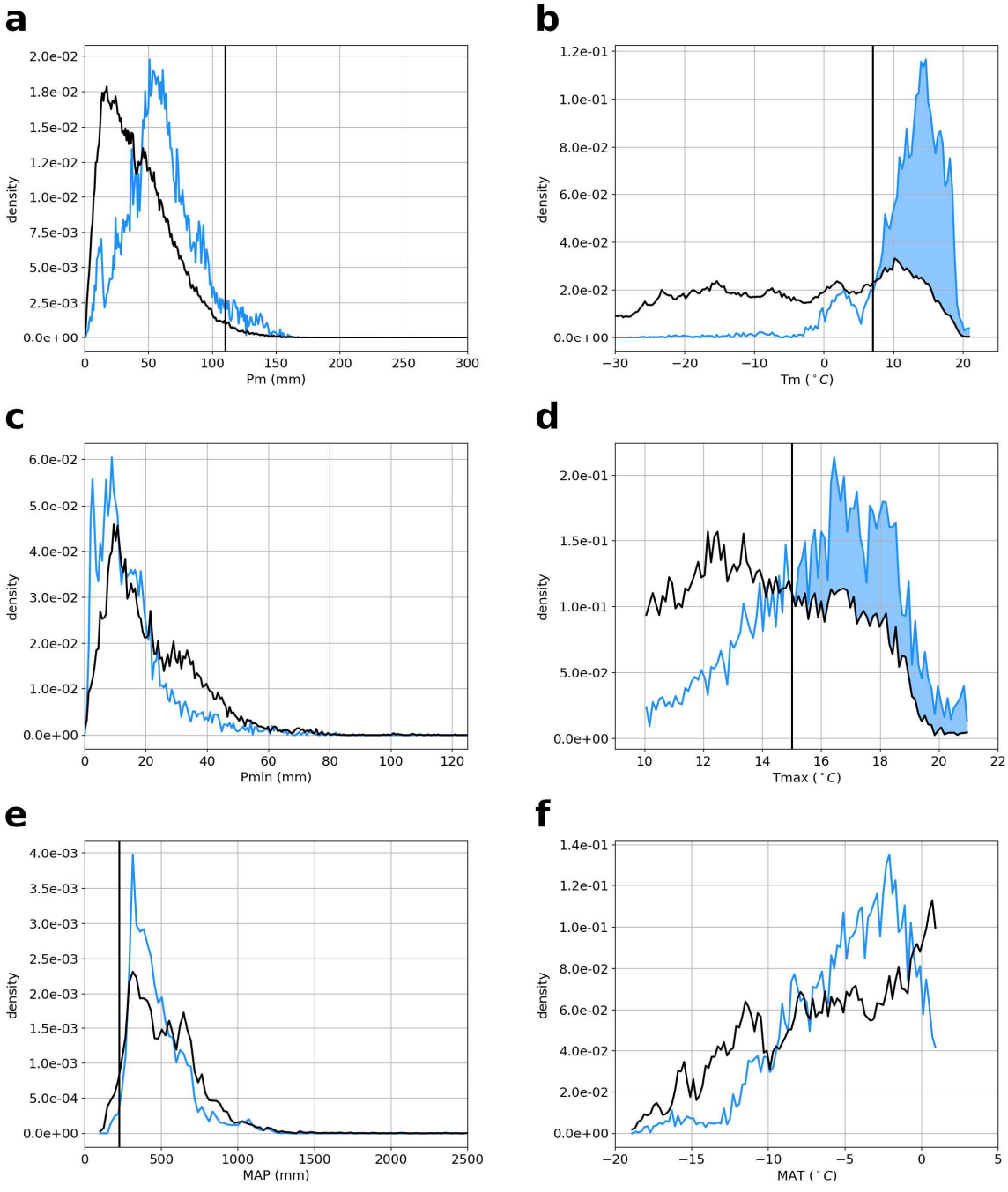

Figure S12. Boreal statistical distributions. Same as Fig. S3 but with cold data. Fire-prone probability density functions are shown in blue.

Fire-climate classification reliability

We note that some fire-impacted areas have not been classified (in grey in Fig 2a). Notwithstanding, they correspond for the most part to areas with relatively low fire incidence, as combined they only account for about 5% of the global mean annual burned area.

Among the unclassified regions, maybe the most notorious is South-Eastern Australia. Australia is sometimes considered the most fire-prone continent[78]. Most of its area is classified as A-ds and B-dhs, with some smaller regions in the C-dhs category. The fire season in the South-Eastern region takes place during summer (Fig. S13), but high precipitation values during these months prevent this area from being classified as C-dhs. In fact, it is a region without a dry season. The monthly burned area time series of Fig. S13 evidences that the fire activity in this Australian region is dominated by a high interannual variability, with much of the mean annual burned area concentrated in just a few months of the entire 1996-2016 period. Fires in the South of Australia are less frequent but more severe[7,78], resulting in high BA values coming from few fires.

Other important fire-prone areas that are not classified in Fig. 2 are located in the Great Plains and South-eastern North America, Eastern China and in a region north of the Black Sea and the Caspian Sea belonging to Ukraine and Russia. The burned area observed in these regions is mainly associated with agricultural management fires in croplands (Supplementary Fig. S1b), despite existent bans on the practice in countries like Russia[70]. Major agricultural regions like the Corn Belt of the U.S., Eastern China, and Southern Australia, where there are areas that display little synchrony between natural eco-climatic seasonality and fire seasonality, present great influence of anthropogenic activities on fire activity[71]. Other regions that are not classified show lower values of mean annual burned area, like the Pampa region or South-eastern Brazil (Supplementary Fig. S14), where the fire activity is low but extended during the whole year. South-eastern maritime Asia (Indonesia, Malaysia and Papua New Guinea) is a region that is regularly not fire-prone, except when fire activity is favoured by inter-annual dry seasons associated with El Niño events, as suggested by the coincidence of low precipitation periods and high fire activity during the El Niño episodes of 1997/1998, 2002/2003, 2009/2010 and 2015/2016[19,79,80] (Fig. S15).

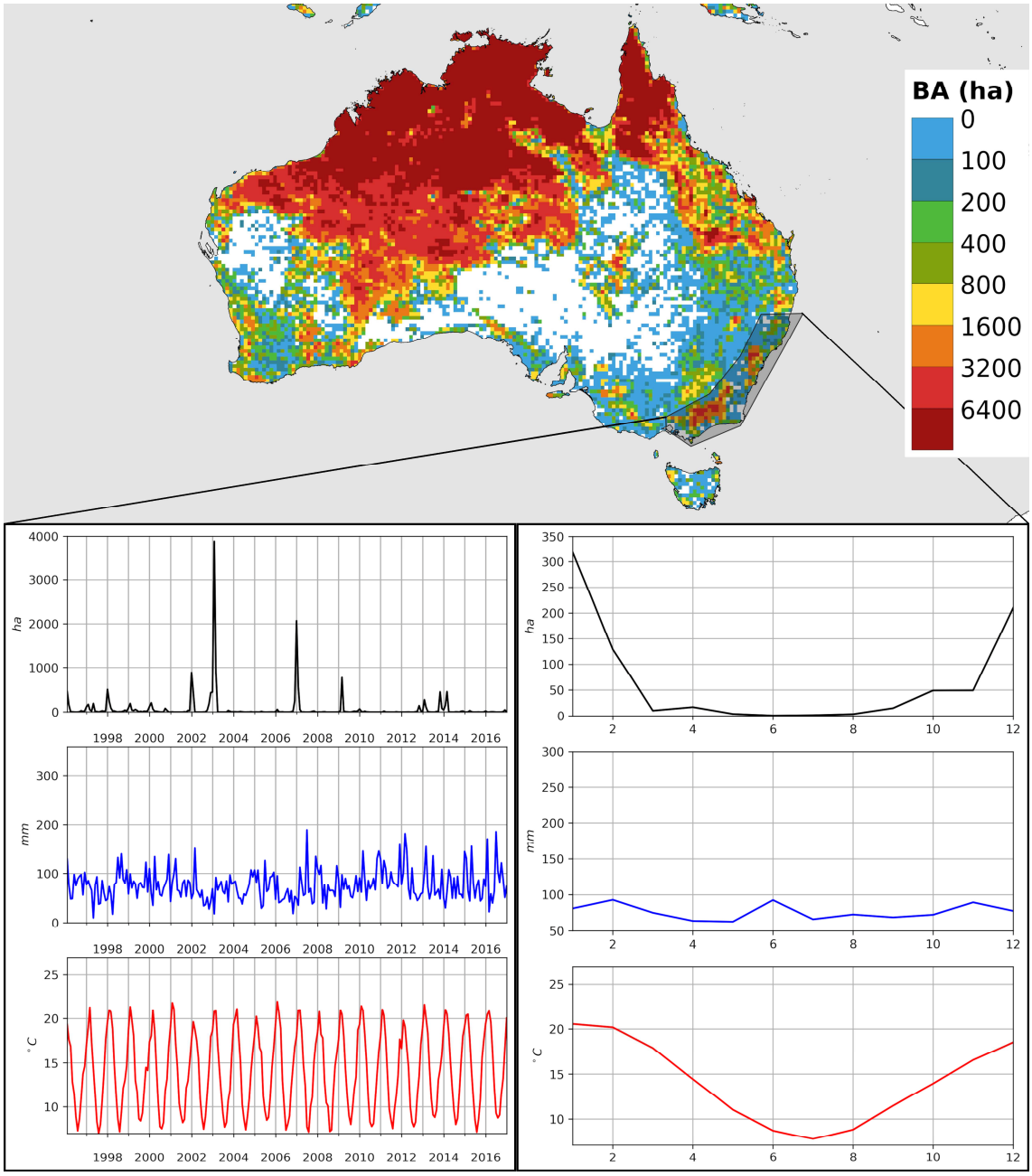

Figure S13. 1996-2016 time series of mean monthly values (a, c, d) and the mean annual cycles (b, d, f) of burned area (a, b, in black), precipitation (c, d, in blue) and 2m air temperature (e, f in red) for the South-eastern Australia fire-prone region (BA>0ha).

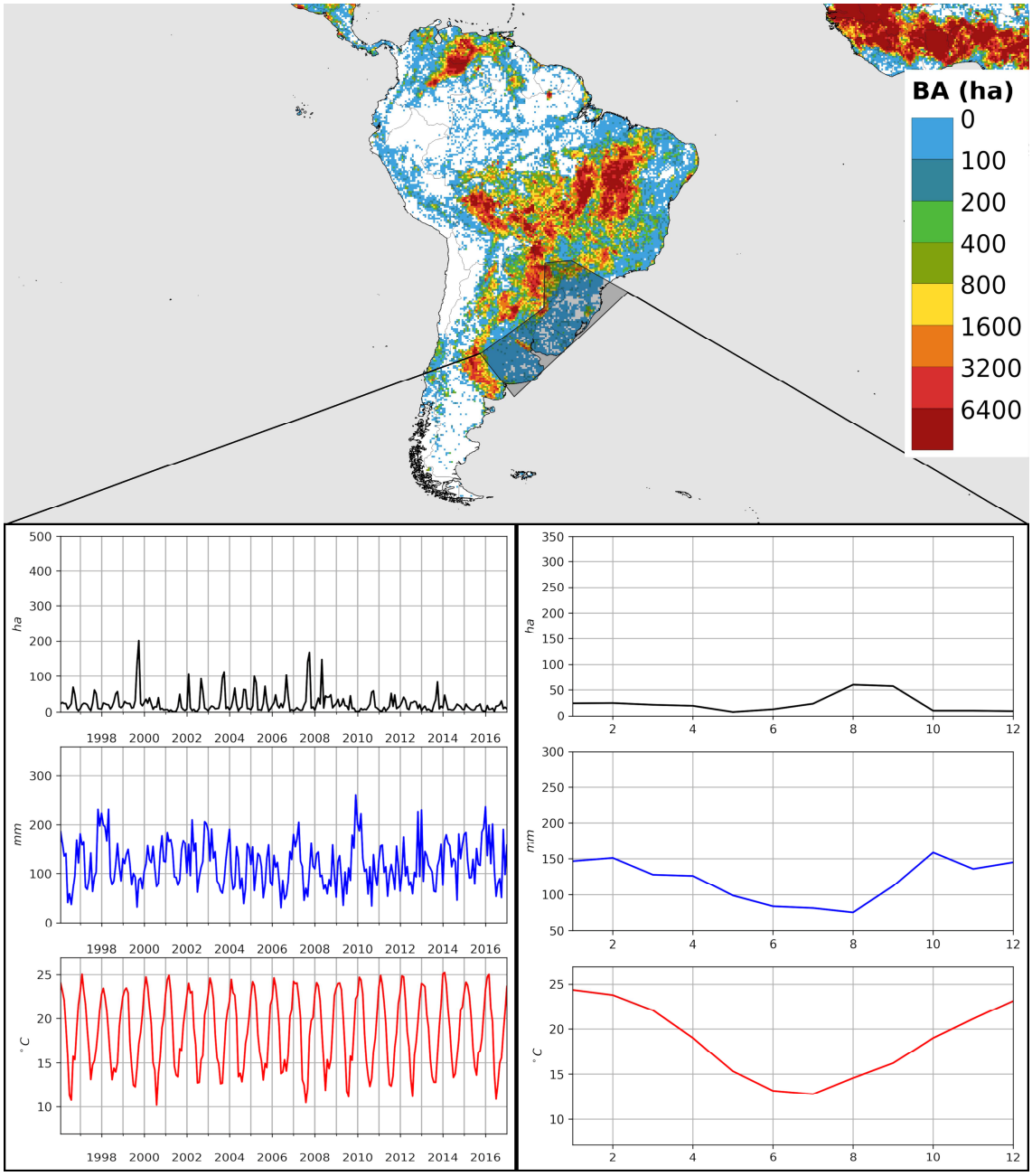

Figure S14. Same as Fig. S13 but for the Pampas and Southern Brazil fire-prone region (BA>0ha).

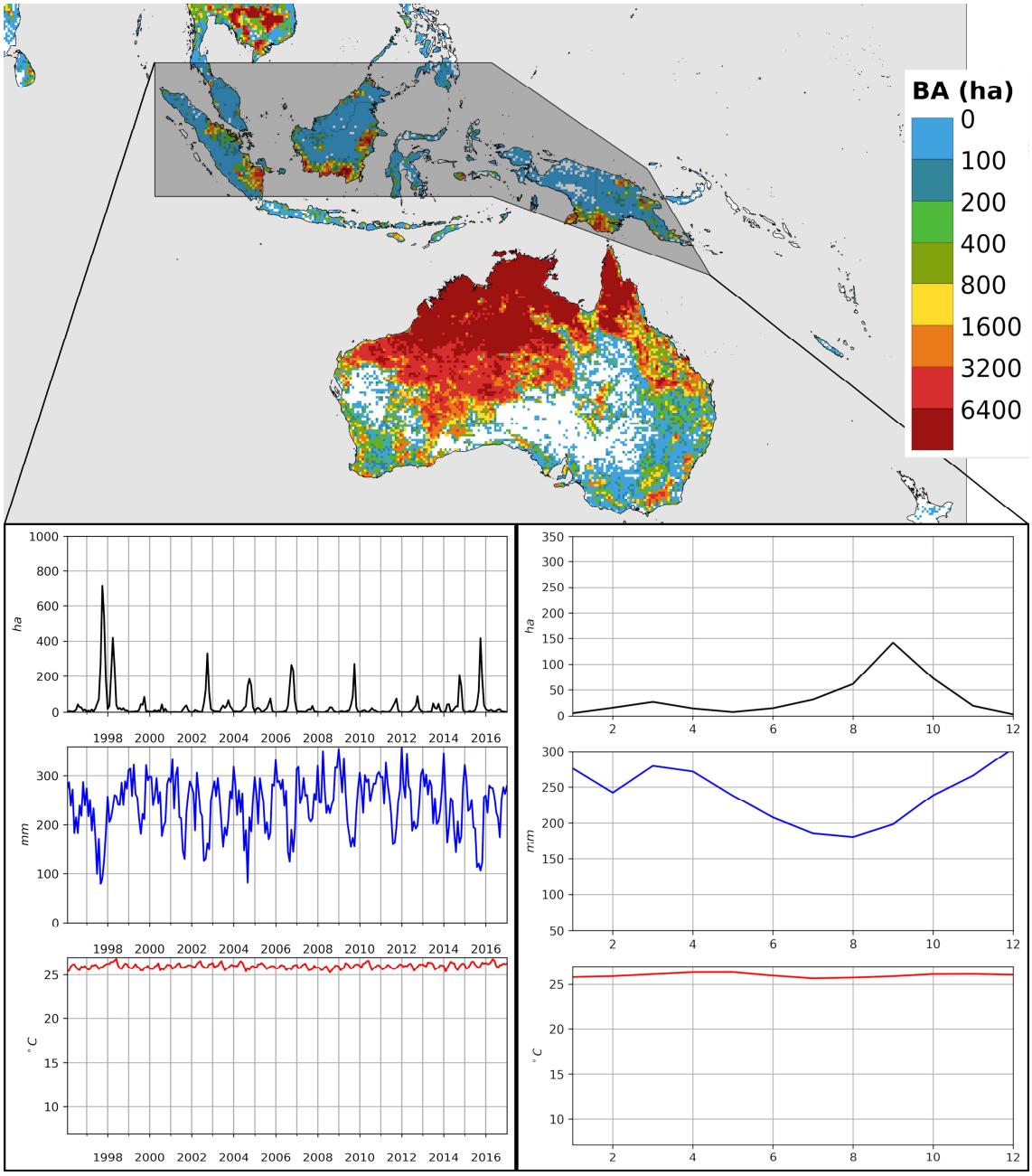

Figure S15. Same as Fig. S14 but for the Malay Archipelago fire-prone region (BA>0ha).

On the contrary, some regions with BA=0ha are classified as fire-prone (in black in Fig. 2a). Most of them correspond to boundaries between arid fire-prone areas (B-dhs) and deserts (e.g. Afghanistan, Ethiopia, Niger or Australia), which are difficult to define based solely on mean annual precipitation. In the Scandinavian Peninsula the burned area data do not reflect high fire activity. However, our classification identifies a fire-prone region from Northwest Russia towards the North of Sweden. The mismatch between our results and the burned area data in

this case could be due to the effective fire suppression system in Nordic countries like Finland[81].

Although there may be coincidences between our climate classification and fire regimes, e.g. infrequent fires in Boreal regions (D-hs) or frequent fires in the Tropics (A-ds)[62], our classification is not related to fire regimes because these are strongly dependent on other factors such as vegetation traits[82] or human action[83].

Future changes in precipitation and temperature

To understand the factors behind the future changes in the spatial expansion of the fire-prone regions and in the length of the potential fire season, we examine the precipitation and temperature differences between future and present data. The global future change projections for mean annual precipitation (MAP) and mean annual temperature (MAT) are shown in Fig. S16. We next focus solely on regions that are classified as fire-prone either at the present, the future or both, and analyse temperature and precipitation changes for their fire season months. Figure S17 shows at any given location, the average changes in precipitation and temperature for the months that are not fire-prone at the present but are projected to become so in the future. If there isn't any expansion of the fire season, the point values are null. Note that some areas do not have any fire activity at the present but conditions for fire will become favourable in the future during some months, and the average changes for those months are shown in the map. Conversely, Fig. S18 represents at any given location, the average changes in precipitation and temperature for the months that presently are but will no longer be fire-prone in the future. For points that have no fire activity at the present, or where the fire season is not projected to reduce in the future, the values are null. Finally, Fig. S19 depicts for any given location, the average changes in precipitation and temperature for the months that are fire prone at the present and will continue to be so in the future. If the point does not have fires in both the present and the future, or if they occur in different months, the values are null.

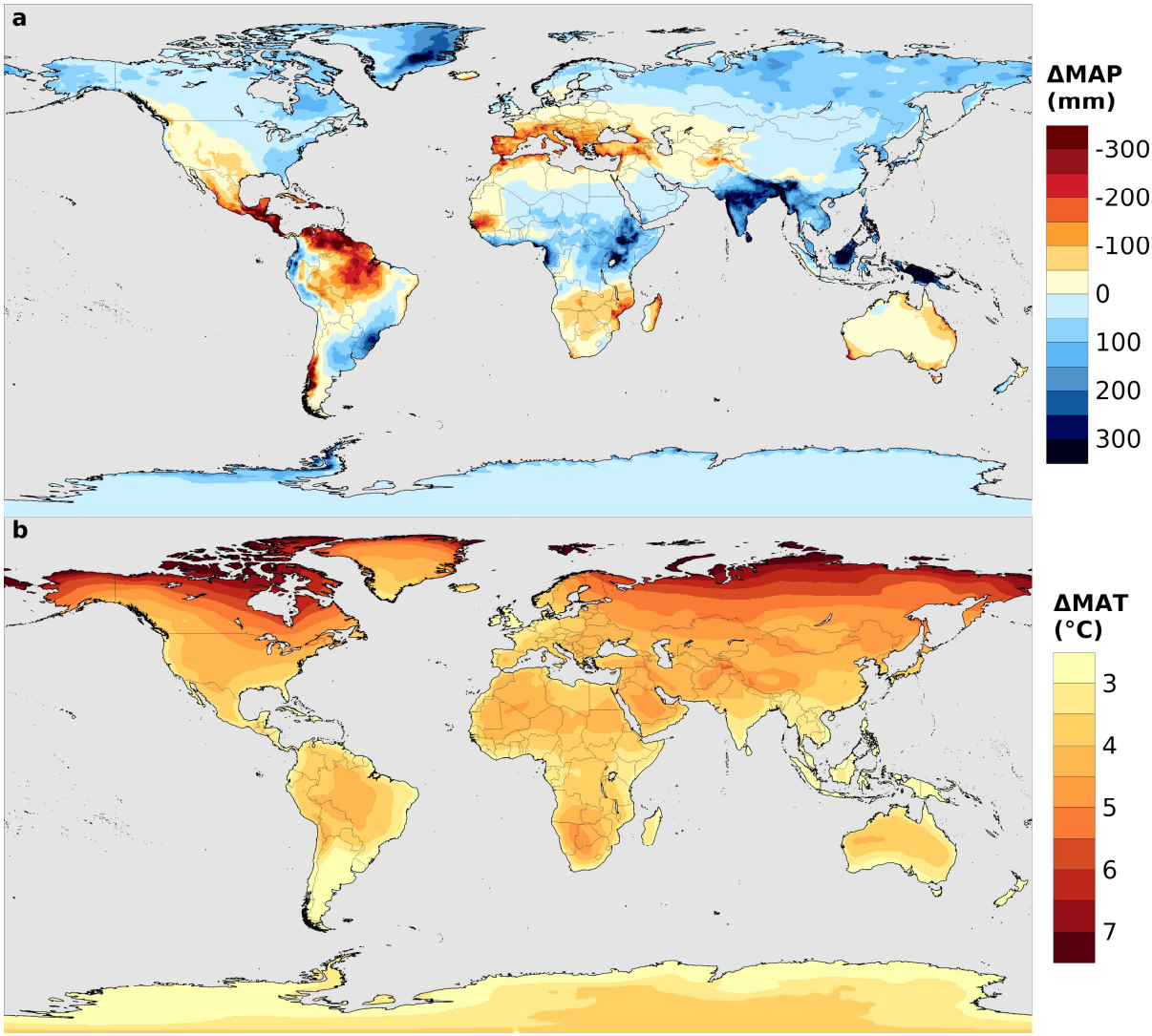

Figure S16. Future changes in annual mean precipitation and temperature. a, Difference between 2070-2099 MAP and 1996-2016 MAP (ΔMAP). **b**, Difference between 2070-2099 MAT and 1996-2016 MAT (ΔMAT).

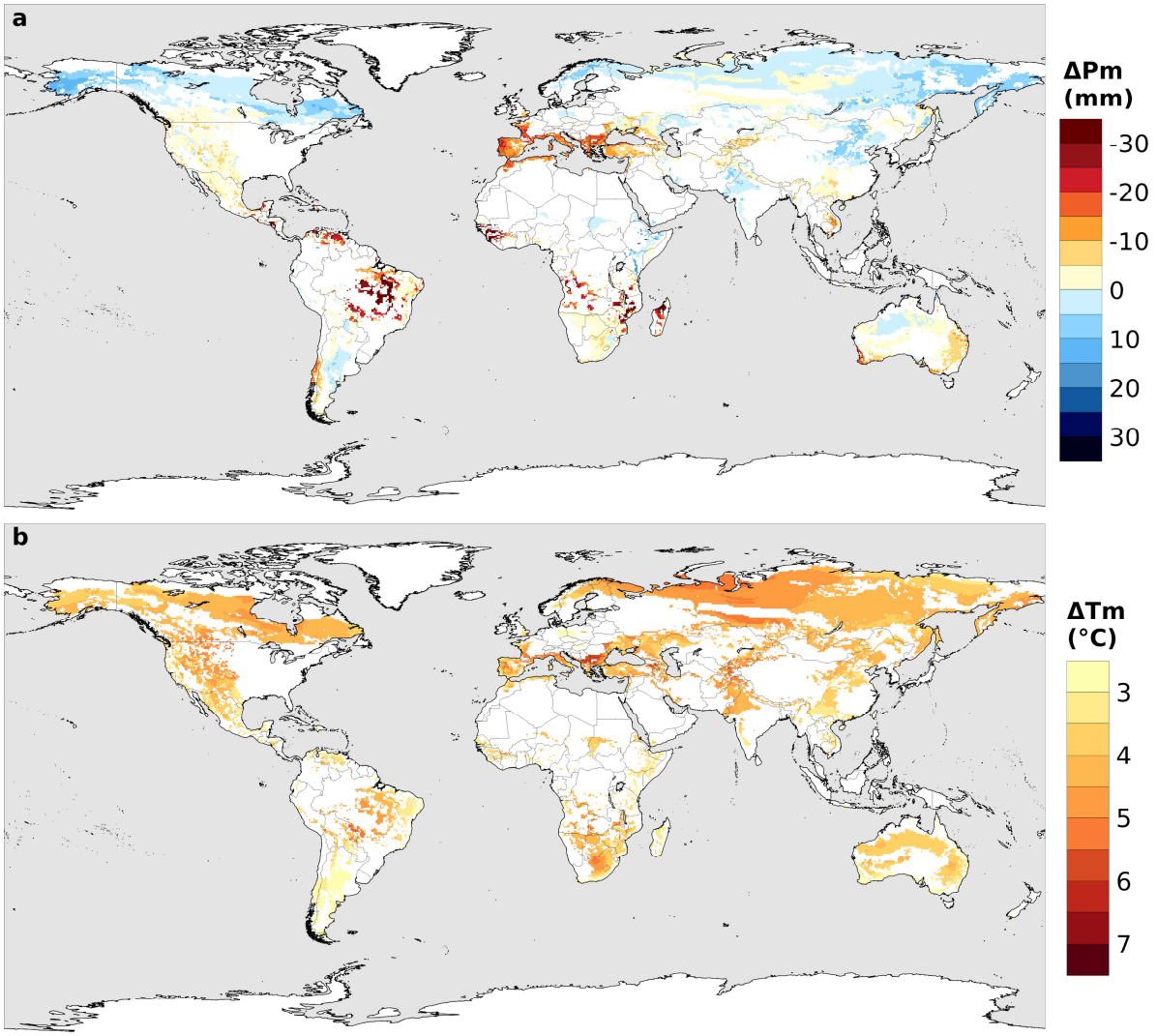

Figure S17. Future changes in precipitation and temperature for the months that are projected to become fire-prone in the future at any given location. a, Difference between 2070-2099 and 1996-2016 mean monthly precipitation for the months that are not classified as fire-prone in the present but are classified as fire-prone in the future, at any given location (ΔPm). **b**, Difference between 2070-2099 and 1996-2016 mean monthly temperature for the months that are not classified as fire-prone in the present but are classified as fire-prone in the future, at any given location (ΔTm).

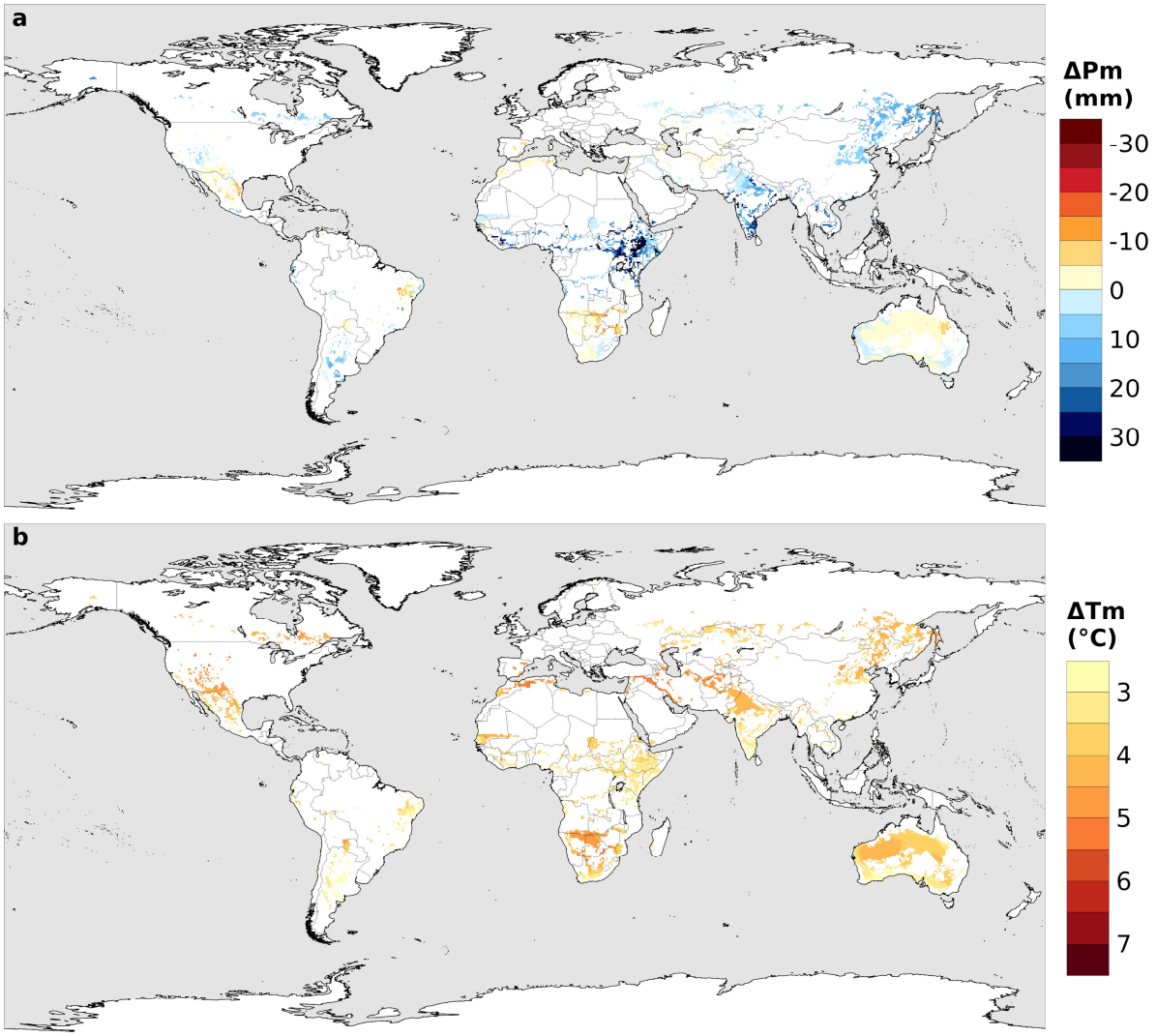

Figure S18. Future changes in precipitation and temperature for the months that are projected to become fireless in the future at any given location. a, Difference between 2070-2099 and 1996-2016 mean monthly precipitation for the months that are classified as fire-prone in the present but are not classified as fire-prone in the future, at any given location (ΔPm). **b**, Difference between 2070-2099 and 1996-2016 mean monthly temperature for the months that are classified as fire-prone in the present but are not classified as fire-prone in the future, at any given location (ΔTm).

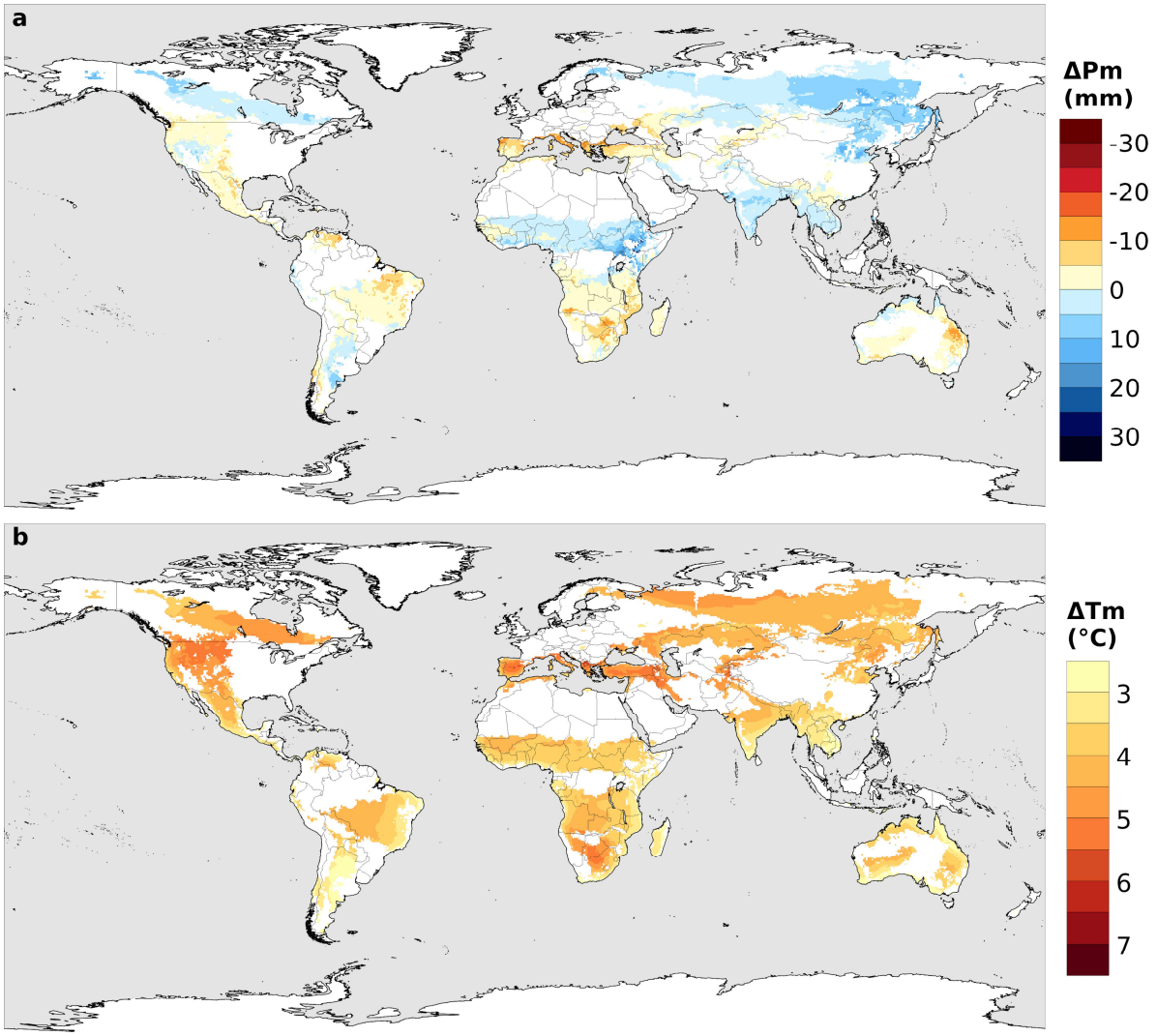

Figure S19. Future changes in precipitation and temperature for the months that are projected to remain fire-prone at any given location. a, Difference between 2070-2099 and 1996-2016 mean monthly precipitation for the months that are classified as fire-prone in both the future and the present, at any given location (ΔPm). **b**, Difference between 2070-2099 and 1996-2016 mean monthly temperature for the months that are classified as fire-prone in both the future and the present, at any given location (ΔTm).

References

1. Andela, N. *et al.* A human-driven decline in global burned area. *Science* **356**, 1356-1362 (2017).
2. Flannigan, M. D., Krawchuk, M. A., de Groot, W. J., Wotton, B. M. & Gowman, L. M. Implications of changing climate for global wildland fire. *Int. J. Wildland Fire* **18**, 483-507 (2009).
3. Bowman, D. M. *et al.* Fire in the Earth system. *Science* **324**, 481-484 (2009).
4. Langmann, B., Duncan, B., Textor, C., Trentmann, J. & Van der Werf, G. R. Vegetation fire emissions and their impact on air pollution and climate. *Atmos. Environ.* **43**, 107-116 (2009).
5. Scholes, R. J. & Archer, S. R. Tree-grass interactions in savannas. *Annu. Rev. Ecol. Syst.* **28**, 517-544 (1997).
6. Cochrane, M. A. Fire science for rainforests. *Nature* **421**, 913-919 (2003).
7. Bowman, D. M. *et al.* Human exposure and sensitivity to globally extreme wildfire events. *Nat. Ecol. Evol.* **1**, 1-6 (2017).
8. Marlon, J. R. *et al.* Global biomass burning: a synthesis and review of Holocene paleofire records and their controls. *Quat. Sci. Rev.* **65**, 5-25 (2013).
9. Aldersley, A., Murray, S. J. & Cornell, S. E. Global and regional analysis of climate and human drivers of wildfire. *Sci. Total Environ.* **409**, 3472-3481 (2011).
10. Jolly, W. M. *et al.* Climate-induced variations in global wildfire danger from 1979 to 2013. *Nat. Commun.* **6**, 1-11 (2015).
11. Krawchuk, M. A. & Moritz, M. A. Constraints on global fire activity vary across a resource gradient. *Ecology* **92**, 121-132 (2011).
12. Krawchuk, M. A., Moritz, M. A., Parisien, M. A., Van Dorn, J. & Hayhoe, K. Global pyrogeography: the current and future distribution of wildfire. *PloS ONE, 4*(4) (2009).
13. Abatzoglou, J. T., Williams, A. P., Boschetti, L., Zubkova, M. & Kolden, C. A. Global patterns of interannual climate–fire relationships. *Glob. Chang. Biol.* **24**, 5164-5175 (2018).
14. Van Der Werf, G. R., Randerson, J. T., Giglio, L., Gobron, N. & Dolman, A. J. Climate controls on the variability of fires in the tropics and subtropics. *Global Biogeochem. Cycles* **22**, GB3028 (2008).
15. Flannigan, M. *et al.* Global wildland fire season severity in the 21st century. *For. Ecol. Manag.* **294**, 54-61 (2013).

16. Liu, Y., Stanturf, J. & Goodrick, S. Trends in global wildfire potential in a changing climate. *For. Ecol. Manag.* **259**, 685-697 (2010).
17. Pechony, O. & Shindell, D. T. Driving forces of global wildfires over the past millennium and the forthcoming century. *Proc. Natl Acad. Sci. USA* **107**, 19167-19170 (2010).
18. Moritz, M. A. *et al.* Climate change and disruptions to global fire activity. *Ecosphere* **3**, 1-22 (2012).
19. Giglio, L., Randerson, J. T. & Van der Werf, G. R. Analysis of daily, monthly, and annual burned area using the fourth-generation global fire emissions database (GFED4). *J. Geophys. Res. Biogeosc.* **118**, 317-328 (2013).
20. Köppen, W. *Das geographische System der Klimate,* 1-44 (Gebrüder Borntraeger: Berlin, Germany, 1936).
21. Cahoon, D. R., Stocks, B. J., Levine, J. S., Cofer, W. R. & O'Neill, K. P. Seasonal distribution of African savanna fires. *Nature* **359**, 812-815 (1992).
22. Archibald, S., Roy, D. P., van Wilgen, B. W., & Scholes, R. J. What limits fire? An examination of drivers of burnt area in Southern Africa. *Glob. Change Biol.* **15**, 613-630 (2009).
23. Van Der Werf, G. R., Randerson, J. T., Collatz, G. J., & Giglio, L. Carbon emissions from fires in tropical and subtropical ecosystems. *Glob. Change Biol.* **9**, 547-562 (2003).
24. Gillett, N. P., Weaver, A. J., Zwiers, F. W. & Flannigan, M. D. Detecting the effect of climate change on Canadian forest fires. *Geophys. Res. Lett.* **31**, L18211 (2004).
25. Flannigan, M. D., Logan, K. A., Amiro, B. D., Skinner, W. R., & Stocks, B. J. Future area burned in Canada. *Clim. Change* **72**, 1-16 (2005).
26. Littell, J. S., McKenzie, D., Peterson, D. L. & Westerling, A. L. Climate and wildfire area burned in western US ecoprovinces, 1916-2003. *Ecol. Appl.* **19**, 1003-1021 (2009).
27. Marlon, J. R. *et al.* Long-term perspective on wildfires in the western USA. *Proc. Natl Acad. Sci. USA* **109**, E535-E543 (2012).
28. Parisien, M. A., & Moritz, M. A. Environmental controls on the distribution of wildfire at multiple spatial scales. *Ecol. Monogr.* **79**, 127-154 (2009).
29. Seager, R. *et al.* Climatology, variability, and trends in the US vapor pressure deficit, an important fire-related meteorological quantity. *J. Appl. Meteor. Climatol.* **54**, 1121-1141 (2015).

30. Sousa, P. M., Trigo, R. M., Pereira, M. G., Bedia, J., & Gutiérrez, J. M. Different approaches to model future burnt area in the Iberian Peninsula. *Agric. For. Meteorol.* **202**, 11-25 (2015).
31. Turco, M. *et al.* On the key role of droughts in the dynamics of summer fires in Mediterranean Europe. *Sci. Rep.* **7**, 1-10 (2017).
32. Hantson, S. *et al*. The status and challenge of global fire modelling. *Biogeosciences*, **13**, 3359-3375 (2016).
33. Nolan, C. *et al.* Past and future global transformation of terrestrial ecosystems under climate change. *Science* **361**, 920-923 (2018).
34. Beck, H. E. *et al.* Present and future Köppen-Geiger climate classification maps at 1-km resolution. *Sci. Data* **5**, 180214 (2018).
35. Bedia, J. *et al.* Global patterns in the sensitivity of burned area to fire-weather: Implications for climate change. *Agric. For. Meteorol.* **214**, 369-379 (2015).
36. Pithan, F. & Mauritsen, T. Arctic amplification dominated by temperature feedbacks in contemporary climate models. *Nat. Geosci.* **7**, 181-184 (2014).
37. Flannigan, M. D. *et al.* Fuel moisture sensitivity to temperature and precipitation: climate change implications. *Clim. Change* **134**, 59-71 (2016).
38. De Groot, W. J., Flannigan, M. D., & Cantin, A. S. Climate change impacts on future boreal fire regimes. *For. Ecol. Manag.* **294**, 35-44 (2013).
39. Giorgi, F. & Lionello, P. Climate change projections for the Mediterranean region. *Glob. Planet. Change* **63**, 90-104 (2008).
40. Abatzoglou, J. T., & Williams, A. P. Impact of anthropogenic climate change on wildfire across western US forests. *Proc. Natl Acad. Sci. USA* **113**, 11770-11775 (2016).
41. Dennison, P. E., Brewer, S. C., Arnold, J. D., & Moritz, M. A. Large wildfire trends in the western United States, 1984–2011. *Geophys. Res. Lett.* **41**, 2928-2933 (2014).
42. Goss, M. *et al.* Climate change is increasing the likelihood of extreme autumn wildfire conditions across California. *Environ. Res. Lett.* **15**, 094016 (2020).
43. Barbero, R., Abatzoglou, J. T., Larkin, N. K., Kolden, C. A. & Stocks, B. Climate change presents increased potential for very large fires in the contiguous United States. *Int. J. Wildland Fire* **24**, 892-899 (2015).
44. Turco, M. *et al.* Exacerbated fires in Mediterranean Europe due to anthropogenic warming projected with non-stationary climate-fire models. *Nature commun.* **9**, 1-9 (2018).

45. Serdeczny, O. *et al.* Climate change impacts in Sub-Saharan Africa: from physical changes to their social repercussions. *Reg. Environ. Change* **17**, 1585-1600 (2017).
46. Andela, N. & Van Der Werf, G. R. Recent trends in African fires driven by cropland expansion and El Nino to La Nina transition. *Nat. Clim. Change* **4**, 791-795 (2014).
47. Dore, M. H. Climate change and changes in global precipitation patterns: what do we know?. *Environ. Int.* **31**, 1167-1181 (2005).
48. Fasullo, J. T., Otto-Bliesner, B. L. & Stevenson, S. ENSO's changing influence on temperature, precipitation, and wildfire in a warming climate. *Geophys. Res. Lett.* **45**, 9216-9225 (2018).
49. Perry, S. J., McGregor, S., Gupta, A. S. & England, M. H. Future changes to El Niño–Southern Oscillation temperature and precipitation teleconnections. *Geophys. Res. Lett.* **44**, 10608-10616 (2017).
50. Van Der Werf *et al*. Global fire emissions estimates during 1997-2016. *Earth Syst. Sci. Data* **9**, 697-720 (2017).
51. Giglio, L., Loboda, T., Roy, D. P., Quayle, B. & Justice, C. O. An active-fire based burned area mapping algorithm for the MODIS sensor. *Remote Sens. Environ.* **113**, 408-420 (2009).
52. Copernicus Climate Change Service (C3S). Near surface meteorological variables from 1979 to 2018 derived from bias-corrected reanalysis. Copernicus Climate Change Service Climate Data Store (CDS). https://doi.org/10.24381/cds.20d54e34 (2020).
53. Copernicus Climate Change Service (C3S). ERA5: Fifth generation of ECMWF atmospheric reanalyses of the global climate. Copernicus Climate Change Service Climate Data Store (CDS). (2017).
54. Weedon, G. P. *et al.* Creation of the WATCH forcing data and its use to assess global and regional reference crop evaporation over land during the twentieth century. *J. Hydrometeorol.* **12**, 823-848 (2011).
55. Cucchi, M. *et al.* WFDE5: bias adjusted ERA5 reanalysis data for impact studies. *Earth Syst. Sci. Data* **12**, 2097–2120 (2020).
56. Harris, I. P. D. J., Jones, P. D., Osborn, T. J. & Lister, D. H. Updated high-resolution grids of monthly climatic observations–the CRU TS3. 10 Dataset. *Int. J. Climatol.* **34**, 623-642 (2014).
57. Schneider, U., Becker, A., Finger, P., Meyer-Christoffer, A. & Ziese, M. GPCC Full Data Reanalysis Version 7.0 at 0.5°: Monthly Land-Surface Precipitation from Rain-Gauges built on GTS-based and Historic Data. Research Data Archive at the National

Center for Atmospheric Research, Computational and Information Systems Laboratory. https://doi.org/10.5065/D6000072 (2015).

58. Taylor, K. E., Stouffer, R. J. & Meehl, G. A. An overview of CMIP5 and the experiment design. *Bull. Amer. Met. Soc.* **93**, 485-498 (2012).

59. Riahi, K. et al. RCP 8.5—A scenario of comparatively high greenhouse gas emissions. *Clim. change* **109**, 33-57 (2011).

60. Van Vuuren, D. P. et al. The representative concentration pathways: an overview. *Clim. change* **109**, 5-31 (2011).

61. Teutschbein, C. & Seibert, J. Bias correction of regional climate model simulations for hydrological climate-change impact studies: Review and evaluation of different methods. *J. Hydrol.* **456**, 12-29 (2012).

62. Archibald, S., Lehmann, C. E., Gómez-Dans, J. L. & Bradstock, R. A. Defining pyromes and global syndromes of fire regimes. *Proc. Natl Acad. Sci. USA* **110,** 6442-6447 (2013).

63. Yue, C. et. al. Modelling the role of fires in the terrestrial carbon balance by incorporating SPITFIRE into the global vegetation model ORCHIDEE-Part 1: Simulating historical global burned area and fire regimes. *Geosci. Model Dev.* **7**, 2747–2767 (2014).

64. Peel, M. C., Finlayson, B. L. & McMahon, T. A. Updated world map of the Köppen-Geiger climate classification. *Hydrology and Earth System Sciences* **11,** 1633-1644 (2007).

65. Wilcock, A. A. Köppen after fifty years. *Annals of the Association of American Geographers* **58,** 12-28 (1968).

66. Russel, R. J. Dry climates of the United States: I. Climatic map. *University of California, Publications in Geography* **5,** 1-41 (1931).

67. Kottek, M., Grieser, J., Beck, C., Rudolf, B., & Rubel, F. World map of the Köppen-Geiger climate classification updated. *Meteorologische Zeitschrift* **15,** 259-263 (2006).

68. Whittaker, R. H. *Communities and Ecosystems.* 2nd ed. 167 (MacMillan, New York, 1975).

69. Woodward, F. I., Lomas, M. R., & Kelly, C. K. Global climate and the distribution of plant biomes. *Philosophical Transactions of the Royal Society of London. Series B: Biological Sciences*, **359,** 1465-1476 (2004).

70. Hall, J. V., Loboda, T. V., Giglio, L., & McCarty, G. W. A MODIS-based burned area assessment for Russian croplands: Mapping requirements and challenges. *Remote Sens. Environ.* **184**, 506-521 (2016).

71. Le Page, Y., Oom, D., Silva, J. M., Jönsson, P., & Pereira, J. M. Seasonality of vegetation fires as modified by human action: Observing the deviation from eco-climatic fire regimes. *Glob. Ecol. Biogeogr.* **19**, 575-588 (2010).
72. Bradstock, R. A. A biogeographic model of fire regimes in Australia: current and future implications. *Glob. Ecol. Biogeogr.* **19**, 145-158 (2010).
73. Pausas, J. G., & Ribeiro, E. The global fire–productivity relationship. *Glob. Ecol. Biogeogr.* **22**, 728-736 (2013).
74. Andela, N. *et al.* Biomass burning fuel consumption dynamics in the tropics and subtropics assessed from satellite. *Biogeosci. Discuss.* **13**, 3717-3734 (2016).
75. Kull, C.A. & Laris, P. Fire ecology and fire politics in Mali and Madagascar. In: *Tropical Fire Ecology: Climate Change, Land Use, and Ecosystem Dynamics.* Ed. Cochrane, M., pp. 171-226 (Springer-Praxis, Heidelberg, 2009).
76. Laris, P. Burning the seasonal mosaic: preventative burning strategies in the wooded savanna of southern Mali. *Hum. Ecol.* **30**, 155-186 (2002).
77. Mbow, C., Nielsen, T. T., & Rasmussen, K. Savanna fires in east-central Senegal: distribution patterns, resource management and perceptions. *Hum. Ecol.* **28**, 561-583 (2000).
78. Murphy, B. P., Prior, L. D., Cochrane, M. A., Williamson, G. J., & Bowman, D. M. Biomass consumption by surface fires across Earth's most fire prone continent. *Glob. Change Biol.* **25**, 254-268 (2019).
79. Van Der Werf, G. R. et al. Continental-scale partitioning of fire emissions during the 1997 to 2001 El Nino/La Nina period. *Science* **303**, 73-76 (2004).
80. Chen, Y. et al. A pan-tropical cascade of fire driven by El Niño/Southern Oscillation. *Nat. Clim. Change* **7**, 906-911 (2017).
81. Kilpeläinen, A., Kellomäki, S., Strandman, H., & Venäläinen, A. Climate change impacts on forest fire potential in boreal conditions in Finland. *Clim. Change* **103**, 383-398 (2010).
82. Archibald, S. et al. Biological and geophysical feedbacks with fire in the Earth system. *Environ. Res. Lett.* **13**, 033003 (2018).
83. Bowman, D. M. et al. The human dimension of fire regimes on Earth. *J. Biogeog.* **38**, 2223-2236 (2011).